



1                   **Revisiting the Steering Principal of Tropical Cyclone Motion**

2

3

4                   Liguang Wu<sup>1,2</sup> and Xiaoyu Chen<sup>1</sup>

5                   <sup>1</sup>Key Laboratory of Meteorological Disaster, Ministry of Education (KLME)/Joint

6                   International Research Laboratory of Climate and Environment Change (ILCEC)

7                   /Collaborative Innovation Center on Forecast and Evaluation of Meteorological

8                   Disasters (CIC-FEMD), Pacific Typhoon Research Center (PTRC), Nanjing

9                   University of Information Science & Technology, Nanjing, China

10                  <sup>2</sup>State Key Laboratory of Severe Weather, Chinese Academy of Meteorological

11                  Sciences, Beijing, China

12

13

14

15

16

17

18                   April 30, 2016

19

20                   Submitted to *Atmospheric Chemistry and Physics*

21

22

23

24                   Corresponding author address: Prof. Liguang Wu

25                   Pacific Typhoon Research Center and Earth System Modeling Center

26                   Nanjing University of Information Science and Technology, Nanjing, Jiangsu 210044,

27                   China

28                   E-mail: [liguang@nuist.edu.cn](mailto:liguang@nuist.edu.cn)



29

### Abstract

30 The steering principle of tropical cyclone motion has been applied to tropical  
31 cyclone forecast and research for nearly 100 years. Two fundamental questions  
32 remain unanswered. One is why the effect of steering plays a dominant role in tropical  
33 cyclone motion and the other is when tropical cyclone motion deviates considerably  
34 from the steering. A high-resolution numerical experiment was conducted with the  
35 tropical cyclone in a typical large-scale monsoon trough over the western North  
36 Pacific. The simulated tropical cyclone experiences two eyewall replacement  
37 processes.

38 Based on the potential vorticity tendency (PVT) paradigm for tropical cyclone  
39 motion, this study demonstrates that the conventional steering, which is calculated  
40 over a certain radius from the tropical cyclone center in the horizontal and a deep  
41 pressure layer in the vertical, is not literally the steering or the advection of the  
42 symmetric potential vorticity component associated with a tropical cyclone by the  
43 asymmetric flow. The conventional steering also contains the contribution from the  
44 advection of the wavenumber-one potential vorticity component by the symmetric  
45 flow. The contributions from other processes are largely cancelled due to the coherent  
46 structure of tropical cyclone circulation and thus the conventional steering plays a  
47 dominant role. The trochoidal motion around the mean tropical cyclone track with  
48 amplitudes smaller than the eye radius and periods of several hours cannot be  
49 accounted for by the effect of the conventional steering and thus the instantaneous  
50 tropical cyclone motion can considerably deviate from the conventional steering.



## 51 1. Introduction

52 The environmental steering principle has been applied to tropical cyclone track  
53 forecasting for nearly 100 years (Fujiwara and Sekiguchi 1919; Bowie 1922), which  
54 states that a tropical cyclone tends to follow the large-scale flow in which it is  
55 embedded. Such a steering concept has been extended to include the secondary  
56 steering (beta drift) that arises mainly from the interaction between tropical cyclone  
57 circulation and the planetary vorticity gradient (Holland 1983; Chan 1984; Chan and  
58 Williams 1987; Fiorino and Elsberry 1989; Carr and Elsberry 1990; and Wang and Li  
59 1992; Wang and Holland 1996a). As a rule of thumb, the steering concept has been  
60 extensively used in tropical cyclone track forecasting and understanding of tropical  
61 cyclone motion (e.g., Simpson 1948; Riehl and Burgner 1950; Chan and Gray 1982;  
62 Fiorino and Elsberry 1989; Neumann 1993; Wu and Emanuel 1995a, b; Wang and  
63 Holland 1996b, c; Wu et al. 2011a; Wu et al. 2011b). Given complicated interactions  
64 between tropical cyclone circulation and its environment, tropical cyclone motion  
65 should be not like a leaf being steered by the currents in the stream. Therefore two  
66 fundamental issues are still remaining on the steering principle. First, why can the  
67 effect of steering play a dominant role in tropical cyclone motion? Second, when may  
68 tropical cyclone motion deviate considerably from the steering?

69 The potential vorticity tendency (PVT) paradigm for tropical cyclone motion was  
70 proposed by Wu and Wang (2000), in which a tropical cyclone tends to move to the  
71 region of the PVT maximum. In other words, tropical cyclone motion is completely  
72 determined by the azimuthal wavenumber-one component of PVT and all of the



73 factors that contribute to the azimuthal wavenumber-one component of PVT play a  
74 potential role in tropical cyclone motion. The individual contributions of these factors  
75 can be quantified through the PVT diagnosis, including the steering effect (Wu and  
76 Wang 2000). Wu and Wang (2000, 2001a) evaluated the PVT approach using the  
77 output of idealized numerical experiments with the coarse spacing of 25 km and  
78 understood the vertical coupling of tropical cyclone circulation under the influence of  
79 vertical wind shear. Wu and Wang (2001b) found that convective heating can affect  
80 tropical cyclone motion by the heating-induced flow and the positive PVT that is  
81 directly generated by convective heating.

82 The PVT paradigm was further verified by Chan et al. (2002). The observational  
83 analysis indicated that the potential vorticity advection process is generally dominant  
84 in tropical cyclone motion without much change in direction or speed while the  
85 contribution by diabatic heating is usually less important. An interesting finding in the  
86 study is that the contribution of diabatic heating becomes important for irregular  
87 tropical cyclone motion, suggesting that track oscillations as well as irregular track  
88 changes may be explained by changes in the convection pattern. The PVT approach  
89 has been used in understanding tropical cyclone motion in the presence of the effects  
90 of land surface friction, river deltas, coastal lines, mountains, islands, cloud-radiative  
91 processes and sea surface pressure gradients (e.g., Wong and Chan 2006; Yu et al.  
92 2007; Fovell et al. 2010; Hsu et al. 2013; Wang et al. 2013; Choi et al. 2013).

93 As we know, the coarse resolution of the numerical experiment in Wu and Wang  
94 (2000) was unable to resolve the eyewall structure and tropical cyclone rainbands,



95 which may affect tropical cyclone motion (Holland and Lander 1993; Nolan et al.  
96 2001; Oda et al. 2006; Hong and Chang 2009). Under the PVT paradigm, in this study  
97 we use the output from a high-resolution numerical experiment to address the  
98 aforementioned two fundamental issues that are important to understanding tropical  
99 cyclone motion. The numerical experiment was conducted with the advanced research  
100 version of the Weather Research and Forecast (ARW-WRF) model. In particular, an  
101 initially symmetric baroclinic vortex is embedded in the low-frequency atmospheric  
102 circulation of Typhoon Matsa (2005) to simulate tropical cyclone motion in a realistic  
103 large-scale environment. For simplicity, the present study focuses on the numerical  
104 experiment without the influences of land surface and topography.

## 105 **2. The output of the numerical experiment**

106 The numerical experiment conducted with the WRF model (version 2.2) in this  
107 study contains five two-way interactive domains. In order to better simulate the  
108 tropical cyclone rainbands and eyewall structure, the horizontal resolutions are 27, 9,  
109 3, 1, 1/3 km, respectively. The outermost domain is centered at 30.0°N, 132.5°E and  
110 the three innermost domains move with the tropical cyclone (Fig. 1). The model  
111 consists of 40 vertical levels with a top of 50 hPa. The WRF single-moment 3-class  
112 scheme and the Kain-Fritsch scheme (Kain and Fritsch 1993) are used in the outmost  
113 domain. The WRF single-moment 6-class scheme (Hong and Lim 2006) and no  
114 cumulus parameterization scheme are used in the four inner domains. The other  
115 model physics options are the Rapid Radiative Transfer Model (RRTM) longwave  
116 radiation scheme (Mlawer et al. 1997), the Dudhia shortwave radiation scheme



117 (Dudhia 1989), and the Yonsei University scheme for planetary boundary layer  
118 parameterization (Noh et al. 2003).

119 The National Centers for Environmental Prediction (NCEP) Final (FNL)  
120 Operational Global Analysis data with resolution of  $1.0^\circ \times 1.0^\circ$  at every 6 h were used  
121 for deriving the large-scale background with a 20-day low-pass Lanczos filter  
122 (Duchon 1979). The low-frequency fields were taken from those of Typhoon Matsa  
123 (2005) from 0000 UTC 5 August to 0000 UTC 9 August 2005. At 0000 UTC 5 August,  
124 the typhoon was located to the northeast of Taiwan Island with the maximum surface  
125 wind of  $45 \text{ m s}^{-1}$ . During the following three days, Matsa moved northwestward in the  
126 monsoon trough and made landfall on mainland China at 1940 UTC 5 August. The  
127 sea surface temperature is spatially uniform being  $29^\circ\text{C}$ . The analysis nudging for the  
128 wind components above the lower boundary layer is used in the coarsest domain to  
129 maintain the large-scale patterns with a nudging coefficient of  $1.5 \times 10^{-4} \text{ s}^{-1}$ .

130 A symmetric vortex is initially embedded at  $25.4^\circ\text{N}$ ,  $123.0^\circ\text{E}$  (Matsa's center) in  
131 the background (Fig. 1). The vortex was spun up for 18 hours on an f-plane without  
132 environmental flows to make it relatively consistent with the WRF model dynamics  
133 and physics. Considering several hours of the initial spin-up, here we focus only on  
134 the 72-hour period from 6 h to 78 h with the output at one-hour intervals. The  
135 simulated tropical cyclone takes a northwest north track (Fig. 1), generally similar to  
136 that of Typhoon Matsa (2005).

137 Figure 2 shows the simulated wind and radar reflectivity fields at 700 hPa after  
138 24-h integration. The vertical wind shear, which is calculated between 200 hPa and



139 850 hPa over a radius of 500 km from the tropical cyclone center, is also plotted in the  
140 figure. The tropical cyclone center is defined as the geometric center of the circle on  
141 which the azimuthal mean tangential wind speed reaches a maximum (Wu et al. 2006).  
142 We use a variational method to determine the tropical cyclone center each hour at  
143 each level. At the time of Figure 2 the vertical wind shear is more than  $10 \text{ m s}^{-1}$ . The  
144 eyewall is open to the southwest and strong eyewall convection occurs mainly on the  
145 downshear left side (Frank and Ritchie 2001). The rainbands simulated in the inner  
146 most domain exhibit apparent cellular structures (Houze 2010), mostly on the eastern  
147 side. Figure 2 suggests that the simulated tropical cyclone has a structure similar to a  
148 typical observed one, especially in the inner core region.

149 Two eyewall replacement processes, which may affect tropical cyclone motion  
150 (Oda et al. 2006; Hong and Chang 2009), are also simulated in the sub-kilometer  
151 resolution experiment. Figure 3 shows the evolution of the azimuthal mean  
152 component of the 700-hPa wind in the 9-km domain. The eyewall replacement  
153 processes take place around 42 h and 68 h, respectively. During the first eyewall  
154 replacement, for example, the wind starts to intensify outside the eyewall around 36 h.  
155 The radius of maximum wind is located at about 40 km after the 6-h spin-up and  
156 decreases to about 30 km at 42 h. We also conducted a similar sensitivity experiment  
157 without the sub-kilometer domain. The tropical cyclone track in the experiment is  
158 generally similar to that in the sub-kilometer simulation, but no eyewall replacement  
159 cycle can be observed in the sensitivity experiment.

### 160 **3. Dominant role of steering in tropical cyclone motion**



161 The relationship between PVT and tropical cyclone motion can be written as (Wu  
162 and Wang 2000)

$$163 \quad \left(\frac{\partial P_1}{\partial t}\right)_f = \left(\frac{\partial P_1}{\partial t}\right)_m - \mathbf{C} \cdot \nabla P_s, \quad (1)$$

164 Where subscripts  $m$  and  $f$  indicate, respectively, the moving and fixed reference frames  
165 and  $\mathbf{C}$  is the velocity of the reference frame that moves with the tropical cyclone. In  
166 other words,  $\mathbf{C}$  is the velocity of tropical cyclone motion, which can vary in the  
167 vertical.  $P_l$  and  $P_s$  are the azimuthal wavenumber-one and symmetric components of  
168 potential vorticity with respect to the storm center. It can be seen that the PVT  
169 generated in the fixed reference frame (the term on the left hand side) is provided for  
170 the development of the wavenumber one component (the first term on the right hand  
171 side) and for tropical cyclone motion (the second term on the right hand side). The  
172 PVT generated in the fixed reference frame can be calculated with the PVT equation  
173 that contains horizontal advection (HA), vertical advection (VA), diabatic heating  
174 (DH) and friction (FR) terms (Wu and Wang 2000). The first term on the right hand  
175 side of Eq. (1) was neglected in Wu and Wang (2000), but we retain it in this study.  
176 The term can be calculated with the two-hour change of the wavenumber one  
177 component in the frame that moves with the tropical cyclone center.

178 Following Wu and Wang (2000), a least square method is used to estimate the  
179 velocity of tropical cyclone motion ( $\mathbf{C}$ ) in Eq. (1). The translation velocity is also  
180 calculated with the hourly positions of the tropical cyclone center. For convenience,  
181 the tropical cyclone motion estimated with the PVT approach and with the center  
182 position is referred to as the PVT velocity and the tropical cyclone velocity,





183 respectively, in the following discussion. In the PVT approach, we find that the  
184 estimated tropical cyclone motion is not much sensitive to the size of the calculation  
185 domain. As we know, however, determination of the steering flow for a given tropical  
186 cyclone is not unique and depends on the size of the calculation domain (Wang et al.  
187 1998). Here we select the calculation domain to minimize the difference between the  
188 tropical cyclone speed and the steering flow. After a series of tests, we find that such a  
189 minimum can be reached when the 850-300hPa layer and 270-km radius are used.  
190 This is consistent with the analysis of the airborne Doppler radar data in Marks et al.  
191 (1992) and Franklin et al (1996). The analysis indicated that tropical cyclone motion  
192 was best correlated with the depth-mean flow averaged over the inner region within 3 °  
193 latitudes.

194 Figure 4a shows the time series of the magnitudes of the tropical cyclone velocity  
195 (black), the PVT velocity (blue) and the effect of steering (red). Note that the PVT  
196 velocity and the effect of steering are instantaneous, whereas the tropical cyclone  
197 velocity is calculated based on the two-hour difference of the center position. For  
198 consistence, a three-point running mean is applied to the PVT speed and steering.  
199 These magnitudes generally increase as the tropical cyclone takes a northwest north  
200 track. The mean speeds calculated from the PVT approach and the center positions are  
201  $2.86 \text{ m s}^{-1}$  and  $2.75 \text{ m s}^{-1}$  over the 72-h period. Compared to the tropical cyclone  
202 speed, the root-mean-square error (RMSE) of the PVT speed is  $0.22 \text{ m s}^{-1}$ , only  
203 accounting for 8% of the tropical cyclone speed.



204        Figures 4b and 4c further display the zonal and meridional components of the  
205 tropical cyclone velocity (black), the PVT velocity (blue) and the effect of steering  
206 (red). While the westward component fluctuates about the mean zonal tropical  
207 cyclone (PVT) speed of  $-1.02$  ( $-1.01$ )  $\text{m s}^{-1}$ , the northward component generally  
208 increases with time. Figure 4 clearly indicates that the translation velocity of the  
209 tropical cyclone can be well estimated with the PVT approach.

210        The environmental and secondary steering flows are indistinctly referred to the  
211 steering flow in this study, which is averaged over the same radius (270 km) as used  
212 in the calculation of the PVT speed. The effects of the steering flow in Fig. 4 are also  
213 averaged over the 850-300 hPa layer. The 72-h mean magnitudes of the tropical  
214 cyclone velocity and steering are  $2.86 \text{ m s}^{-1}$  and  $2.87 \text{ m s}^{-1}$ , respectively, only with a  
215 difference of  $6.7^\circ$  in the motion direction. We also calculated the RMSE of the  
216 steering averaged over various time periods (Fig. 5). The RMSE of the magnitude  
217 decreases with the increasing average period, generally less than 9% of the translation  
218 speed of the tropical cyclone. The difference in direction also decreases with the  
219 increasing average period within 9-11 degrees. Considering uncertainties in  
220 determining tropical cyclone centers and calculating the steering, we conclude that the  
221 steering plays a dominant role in tropical cyclone motion. However, Figure 4  
222 indicates that the instantaneous tropical cyclone motion can considerably deviate  
223 from the conventional steering. The effect of the steering cannot account for the  
224 fluctuations in tropical cyclone motion, which will be further discussed in Section 5.

#### 225    **4. Contributions of individual processes**



226 The individual contributions of various terms in the PVT equation to tropical  
227 cyclone motion can also be estimated with Eq. (1), as shown by Wu and Wang (2000).  
228 In this study, the contribution of the friction (FR) term is calculated as the residual of  
229 the PVT equation. Figure 6 shows the individual contributions of the terms in the  
230 PVT equation to tropical cyclone motion. While the contribution of the HA term plays  
231 a dominant role (Fig. 6c), the figure exhibits considerable fluctuations, suggesting that  
232 the contributions of the DH and VA terms tend to cancel each other (Figs. 6a and 6b).  
233 Here we discuss the contribution of each term in the PVT equation to understand the  
234 dominant role of the steering in tropical cyclone motion.

#### 235 **a. Horizontal advection**

236 As discussed in Wu and Wang (2001b), the HA term in the PVT equation can be  
237 approximately written as:  $-V_1 \cdot \nabla P_s - V_s \cdot \nabla P_1$ , where  $V_s$  is the symmetric component  
238 of the tangential wind and  $V_1$  is the wavenumber-one component of the asymmetric  
239 wind. The first term (HA1) represents the advection of the symmetric potential  
240 vorticity component by the asymmetric flow. The second term is the advection of the  
241 wavenumber-one potential vorticity component by the symmetric flow (HA2). The  
242 contribution of the HA1 term is literally the steering effect.

243 However, the contribution of the HA1 term is not the conventional steering. The  
244 conventional steering is calculated as the velocity of the mean wind averaged over  
245 300-850 hPa within the radius of 270 km from the tropical cyclone center in this study.  
246 For convenience, it is referred to as the conventional steering, while the contribution  
247 of the HA1 term is called the steering in the following discussion. Wu and Wang



248 (2001a) pointed out that the steering effect of HA1 is associated also with the gradient  
249 of the symmetric potential vorticity component, which make its contribution be  
250 confined to the inner region of tropical cyclones.

251 Figure 7 shows the contributions of the HA1 and HA2 terms, which exhibit  
252 considerable fluctuations with time. The contribution of HA and the conventional  
253 steering are also plotted. For clarity, the conventional steering is removed from the  
254 contribution of HA1. The 72-hour mean difference between the HA1 contribution and  
255 the conventional steering is  $-1.25 \text{ m s}^{-1}$  in the zonal component and  $1.62 \text{ m s}^{-1}$  in the  
256 meridional component, suggesting that the contribution of the HA1 term is  
257 considerably different from the conventional steering. In fact, the contributions of the  
258 HA1 and HA2 terms are highly correlated. The correlations for the zonal and  
259 meridional components are  $-0.82$  and  $-0.80$ , respectively. The negative correlations  
260 suggest the cancellation between the contributions of the HA1 and HA2 terms. As a  
261 result, the combined effect of the HA1 and HA2 terms can actually account for the  
262 effect of the conventional steering except the short-time fluctuations, as shown in Fig.  
263 7.

264 The cancellation between the contributions of the HA1 and HA2 terms arises  
265 from the interaction between the symmetric and wavenumber-one components of the  
266 tropical cyclone circulation. As an example, Figure 8a shows HA1 and the  
267 wavenumber-one components of potential vorticity (contours) and winds at 700 hPa  
268 after 18 hours of the integration. The positive (negative) anomalies of potential  
269 vorticity are nearly collocated with the cyclonic (anticyclonic) circulation. Since the



270 potential vorticity in the inner core is generally elevated, the advection of the  
271 symmetric potential vorticity component by the flows between the cyclonic and  
272 anticyclonic circulations leads to the maximum (minimum) HA1 in the exit (entrance)  
273 of the flows between the cyclonic and anticyclonic circulation. On the other hand, the  
274 advection of the wavenumber-one component of potential vorticity by the symmetric  
275 cyclonic flow leads to the maximum HA2 in the entrance and the minimum HA1 in  
276 the exit (Fig. 8b). Although the contributions of the HA1 and HA2 terms can fluctuate  
277 with a magnitude of about  $4 \text{ m s}^{-1}$  (Fig. 7), their combined effect shows only  
278 small-amplitude fluctuations in the tropical cyclone motion. The short-time  
279 fluctuations will be discussed in the next section.

#### 280 **b. Contributions of diabatic heating and vertical advection**

281 Some individual contributions in Figs. 6a and 6b are statistically correlated. For  
282 example, the zonal contribution of the HA term is negatively correlated with that of  
283 the DH term with a coefficients of -0.44, and the meridional contribution of the HA  
284 term is negatively correlated with that of the VA terms with a coefficients of -0.54. It  
285 is suggested that these individual contributions can cancel each other due to the  
286 coherent structure of the tropical cyclone.

287 We first discuss the contribution of the VA term. The VA contains two primary  
288 terms: the advection of the wavenumber-one component of potential vorticity by the  
289 symmetric component of vertical motion (VA1) and the advection of the symmetric  
290 component of potential vorticity by the wavenumber-one component of vertical  
291 motion (VA2). Our examination indicates that the contribution of the VA term is



292 dominated by that of VA2. That is, the direction of the contribution of the VA term is  
293 determined by the orientation of the wavenumber-one component of vertical motion.  
294 Figure 9 shows the wavenumber-one components of the 500-hPa vertical motion,  
295 700-hPa winds relative to tropical cyclone motion, and 500-hPa heating rate after 18  
296 hours of integration. We can see that the upward (downward) motion generally occurs  
297 in the entrance (exit) region of the 700-hPa winds. Bender (1997) found that vorticity  
298 stretching and compression is closely associated with the vorticity advection due to  
299 the relative flow (difference between the wavenumber-one flow and the TC motion).  
300 The vorticity stretching leads to upward vertical motion and convective heating in the  
301 entrance region (Fig. 9). Thus the contribution of the HA term is negatively correlated  
302 with those of the VA and DH terms.

303 The contribution of diabatic heating results mainly from  $-q_s \cdot \nabla_3 h_1$ , where  $q_s$   
304 is the symmetric component of the absolute vorticity,  $\nabla_3$  the three-dimensional  
305 gradient operator,  $h_1$  the wavenumber-one component of diabatic heating rate. Since  
306 the absolute vorticity is dominated by the vertical component of relative vorticity and  
307 diabatic heating rate reaches its maximum in the middle troposphere, it is conceivable  
308 that the contribution of diabatic heating should cancel each other in the low and upper  
309 troposphere. Figure 10 shows the contribution of diabatic heating at 700 hPa and 400  
310 hPa. The correlation between 700 hPa and 400 hPa is -0.68 in the zonal direction and  
311 -0.67 in the meridional direction.

## 312 **5. Trochoidal motion**



313 As shown in Fig. 4, the tropical cyclone motion exhibits considerable fluctuations.  
314 In an instant, the steering can significantly deviate from the tropical cyclone motion.  
315 At 60 h, for example, the zonal steering is  $-0.55 \text{ m s}^{-1}$ , about one third of the zonal  
316 motion of the tropical cyclone ( $-1.42 \text{ m s}^{-1}$ ); The meridional steering is  $2.71 \text{ m s}^{-1}$ ,  
317 slower than the meridional motion of the tropical cyclone ( $3.05 \text{ m s}^{-1}$ ). The deviation  
318 from the tropical cyclone speed is  $13.5^\circ$  in the direction and 18% in the magnitude. It  
319 is clear that the instantaneous velocity of tropical cyclone motion can considerably  
320 deviate from the effect of steering.

321 Based on radar data and satellite images, many studies documented the oscillation  
322 of a tropical cyclone track with respect to its mean motion vector (e. g., Jordan and  
323 Stowell 1955; Lawrence and Mayfield 1977; Muramatsu 1986; Itano et al. 2002;  
324 Hong and Chang 2005). The periods of track oscillations range less than an hour to a  
325 few days (Holland and Lander 1993). In this study, the small-scale oscillation with  
326 amplitudes of that comparable to the eye size and periods of several hours is referred  
327 to as the trochoidal motion of the tropical cyclone center. Willoughby (1988) showed  
328 that a pair of rotating mass and source could lead to trochoidal motion with periods  
329 ranging from 2-10 hours. Flatau and Stevens (1993) argued that wavenumber-one  
330 instabilities in the outflow layer of tropical cyclones could cause trochoidal motion.  
331 Nolan et al. (2001) found that the small-amplitude trochoidal motion is associated  
332 with the instability of the wavenumber-one component of tropical cyclone circulation  
333 due to the presence of the low-vorticity eye. The instability in their three-dimensional  
334 simulation with a baroclinic vortex quickly led to substantial inner-core vorticity



335 redistribution and mixing, displacing the vortex center that rotates around the vortex  
336 core. Our spectral analysis indicates two peaks of the fluctuations of the tropical  
337 cyclone motion centered at 5 hours and 9 hours (Figure not shown), suggesting that  
338 the trochoidal motion is simulated in our high-resolution numerical simulation.

339 Figure 11 shows the oscillation of the tropical cyclone track with respect to the  
340 9-hour running mean track for the periods 6-18 h and 59-70 h. We can see that the  
341 displacement from the mean track is usually less than 6 km with a period of several  
342 hours in this study. This displacement is less than the size of the tropical cyclone eye.  
343 In general, the tropical cyclone centers rotate cyclonically around the mean track, in  
344 agreement with previous observational and numerical studies (Lawrence and  
345 Mayfield 1977; Muramatsu 1986; Itano et al. 2002; Willoughby 1988; Nolan et al.  
346 2001). In association with the trochoidal motion of the tropical cyclone center, as  
347 suggested by Nolan et al. (2001), substantial potential vorticity redistribution and  
348 mixing can be observed in the inner core region (Fig. 12). During the period of 13-18  
349 hours, the tropical cyclone eye generally looks like a triangle, but the orientation of  
350 the triangle changes rapidly, suggesting the potential vorticity redistribution and  
351 mixing in the eye.

352 The trochoidal motion is well indicated in the translation speed estimated with the  
353 PVT approach. Figure 13a shows the fluctuations of tropical cyclone speed, the PVT  
354 speed, and the difference between the tropical cyclone speed and the conventional  
355 steering, in which the 9-hour running mean has been removed. We can see that the  
356 fluctuations of tropical cyclone motion are well represented in the PVT speed.





357 Moreover, the consistence between the fluctuations of tropical cyclone motion and  
358 those with the conventional steering removed suggests that the small-amplitude  
359 oscillation of the tropical cyclone motion cannot be accounted for by the conventional  
360 steering. Figure 13b further compares the time series of tropical cyclone motion  
361 relative to the conventional steering with the time series of the contribution of the HA  
362 term relative to the conventional steering. The two time series are correlated with a  
363 coefficient of 0.60. We can see that the contribution of the HA term plays an  
364 important role in the fluctuations. Since the non-steering effect can well account for  
365 the fluctuations (Fig. 13a), Figure 13b suggests that the VA and DH tend to reduce the  
366 magnitude of the fluctuations.

## 367 **6. Summary**

368 In this study, we addressed two fundamental questions regarding the steering  
369 principle that has been widely applied to tropical cyclone forecast and research for  
370 about a century (Fujiwara and Sekiguchi 1919; Bowie 1922). One is when the effect  
371 of steering play a dominant role in tropical cyclone motion and the other is when  
372 tropical cyclone motion deviates considerably from the steering. The PVT diagnosis  
373 approach proposed by Wu and Wang (2000) is used with the output from a  
374 high-resolution numerical experiment. It is found that the PVT approach can well  
375 estimate tropical cyclone motion, including the small-amplitude trochoidal motion  
376 relative to the mean tropical cyclone track.

377 The effect of the conventional steering flow that is averaged over a certain radius  
378 from the tropical cyclone center and a deep pressure layer (e.g., 850-300 hPa) actually



379 represents the contributions from both of the advection of the symmetric potential  
380 vorticity component by the asymmetric flow (HA1) and the advection of the  
381 wavenumber-one potential vorticity component by the symmetric flow (HA2),  
382 although the contribution of the HA1 term is literally the effect of steering (Wu and  
383 Wang 2001a, 2001b). Due to the coherent structure of tropical cyclone circulation, the  
384 contributions of the HA1 and HA2 terms are highly correlated and the effects of  
385 diabatic heating and vertical advection on tropical cyclone motion are largely  
386 canceled. The instantaneous speed of tropical cyclone motion can considerably  
387 deviate from the conventional steering, while the latter better represents tropical  
388 cyclone motion when averaged over a reasonable time period.

389 The trochoidal motion of the tropical cyclone center is simulated in the numerical  
390 experiment with amplitudes smaller than the eye radius and periods of several hours.  
391 The tropical cyclone center rotates cyclonically around the mean track, in agreement  
392 with previous observational and numerical studies (Lawrence and Mayfield 1977;  
393 Muramatsu 1986; Itano et al. 2002; Willoughby 1988; Nolan et al. 2001). It is found  
394 that the small-amplitude trochoidal motion cannot be accounted for by the effect of  
395 the conventional steering although the contribution of the HA term plays an important  
396 role in the fluctuations. In agreement with previous studies (Willoughby 1988; Nolan  
397 et al. 2001), we suggest that the small-amplitude trochoidal motion results from the  
398 asymmetric dynamics of the tropical cyclone inner core.

399

400 **Acknowledgements.** Many thanks go to Dr. Christopher W. Landsea of the National



401 Hurricane Center for providing us the early references on the steering principle. This  
402 research was jointly supported by the National Basic Research Program of China  
403 (2013CB430103, 2015CB452803), the National Natural Science Foundation of China  
404 (Grant No. 41275093), and the project of the specially-appointed professorship of  
405 Jiangsu Province.

406

407 **References:**

408 Bender, M. A., 1997: The effect of relative flow on the asymmetric structure in the  
409 interior of hurricanes. *J. Atmos. Sci.*, **54**, 703–724.

410 Bowie, E. H., 1922: Formation and movement of West Indian hurricanes. *Mon. Wea.*  
411 *Rev.*, **50**, 173-179.

412 Carr, L. E., and R. L. Elsberry, 1990: Observational evidence for predictions of  
413 tropical cyclone propagation relative to steering. *J. Atmos. Sci.*, **47**, 542–546.

414 Chan, J. C. -L., F. M. F. Ko, and Y. M. Lei, 2002: Relationship between potential  
415 vorticity tendency and tropical cyclone motion. *J. Atmos. Sci.*, **59**, 1317-1336.

416 Chan, J. C. -L., and W. M. Gray, 1982: Tropical cyclone motion and surrounding flow  
417 relationship. *Mon. Wea. Rev.*, **110**, 1354-1374.

418 Chan, J. C. -L., 1984: An observational study of physical processes responsible for  
419 tropical cyclone motion. *J. Atmos. Sci.*, **41**, 1036-1048.

420 Chan, J. C-L., and R. T. Williams, 1987: Analytical and numerical studies of  
421 beta-effect in tropical cyclone motion. Part I: Zero mean flow. *J. Atmos. Sci.*, **44**,  
422 1257–1265.



- 423 Choi, Y., K.-S. Yun, K.-J. Ha, K.-Y. Kim, S.-J. Yoon, J.-C.-L. Chan, 2013: Effects of  
424 Asymmetric SST Distribution on Straight-Moving Typhoon Ewiniar (2006) and  
425 Recurring Typhoon Maemi (2003). *Mon. Wea. Rev.* **141**, 3950-3967.
- 426 Duchon, C. E., 1979: Lanczos filtering in one and two dimensions. *J. Appl. Meteor.*, **18**,  
427 1016–1022.
- 428 Dudhia, J., 1989: Numerical study of convection observed during the winter monsoon  
429 experiment using a mesoscale two-dimensional model. *J. Atmos. Sci.*, **46**,  
430 3077-3107.
- 431 Flatau, M., W. H. Schubert, and D. E. Stevens, 1994: The role of baroclinic processes  
432 in tropical cyclone motion: The influence of vertical tilt. *J. Atmos. Sci.*, **51**,  
433 2589–2601.
- 434 Fiorino, M., and R. L. Elsberry, 1989: Some aspects of vortex structure related to  
435 tropical cyclone motion. *J. Atmos. Sci.*, **46**, 975-990.
- 436 Fovell, R. G., K. L. Corbosiero, A. Seifert, and K.-N. Liou, 2010: Impact of  
437 cloud-radiative processes on hurricane track, *Geophys. Res. Lett.*, **37**, L07808,  
438 doi:10.1029/2010GL042691.
- 439 Frank, W., and E. A. Ritchie, 2001: Effects of vertical wind shear on the intensity and  
440 structure of numerically simulated hurricanes. *Mon. Wea. Rev.*, **129**, 2249–2269.
- 441 Franklin, J. L., S. E. Feuer, J. Kaplan, and S. D. Aberson, 1996: Tropical cyclone  
442 motion and surrounding flow relationship: Searching for beta gyres in Omega  
443 dropwindsonde datasets. *Mon. Wea. Rev.*, **124**, 64–84.
- 444 Fujiwhara, S., and K. Sekiguchi, 1919: Estimated 300 m isobars and the weather of



- 445 Japan. *J. Meteor. Soc. Japan*, **38**, 254-259 (in Japanese).
- 446 Holland, G. J., 1983: Tropical cyclone motion: Environmental interaction plus a beta  
447 effect. *J. Atmos. Sci.*, **40**, 328–342.
- 448 Houze, R.A., 2010: Clouds in tropical cyclones. *Mon. Wea. Rev.*, **138**, 293–344.
- 449 Hsu, L.-H., Hung-Chi Kuo, Robert G. Fovell, 2013: On the Geographic Asymmetry  
450 of Typhoon Translation Speed across the Mountainous Island of Taiwan. *J.*  
451 *Atmos. Sci.* **70**, 1006-1022.
- 452 Itano, T., G. Naito, and M. Oda, 2002: Analysis of elliptical eye of Typhoon Herb  
453 (T9609) (in Japanese with English abstract). *Sci. Eng. Rep. Natl. Def. Acad.*, **39**,  
454 9–17.
- 455 Kain, J. S., and J. M. Fritch, 1993: Convective parameterization for mesoscale models:  
456 the Kain-Fritch scheme. The representation of cumulus convection in numerical  
457 models. *Meteorological Monographs*, **46**, 165-170.
- 458 Lawrence, M. B., and B. M. Mayfield, 1977: Satellite observations of trochoidal  
459 motion during Hurricane Belle 1976. *Mon. Wea. Rev.*, **105**, 1458–1461.
- 460 Marks, F. D., Jr., R. A. Houze, Jr., and J. F. Gamache, 1992: Dual-aircraft  
461 investigation of the inner core of Hurricane Norbert. Part I: Kinematic structure.  
462 *J. Atmos. Sci.*, **49**, 919–942.
- 463 Mlawer, E. J., S. J. Taobman, P. D. Brown, M. J. Iacono, and S. A. Clough, 1997:  
464 Radiative transfer for inhomogeneous atmosphere: RRTM, a validated  
465 correlated-k model for the longwave. *J. Geophys. Res.*, **102**, 16663-16682.
- 466 Muramatsu, T., 1986: Trochoidal motion of the eye of Typhoon 8019. *J. Meteor. Soc.*



- 467            *Japan*, **64**, 259–272.
- 468    Noh, Y., W. G. Cheon, S.-Y. Hong, and S. Raasch, 2003: Improvement of the
- 469            K-profile model for the planetary boundary layer based on large eddy simulation
- 470            data. *Bound.-Layer Meteor.*, **107**, 401–427.
- 471    Neumann, C. J., 1993: Global overview. *Global Guide to Tropical Cyclone*
- 472            *Forecasting*, World Meteor. Org., 1.1–1.56.
- 473    Nolan, D. S., M. T. Montgomery, and L. D. Grasso, 2001: The wavenumber-one
- 474            instability and trochoidal motion of hurricane-like vortices. *J. Atmos. Sci.*, **58**,
- 475            3243–3270.
- 476    Riehl, H., and N. M. Burgner, 1950: Further studies on the movement and formation
- 477            of hurricanes and their forecasting. *Bull. Amer. Meteor. Soc.*, **31**, 244–253.
- 478    Simpson, R. H., 1946: On the movement of tropical cyclones. *Trans. Amer. Geophys.*
- 479            *Union*, **27**, 641–655.
- 480    Wang, B., and X. Li, 1992: The beta drift of three-dimensional vortices: A numerical
- 481            study. *Mon. Wea. Rev.*, **120**, 579–593.
- 482    Wang, B., R. L. Elsberry, Y. Wang, and L. Wu, 1998: Dynamics of tropical cyclone
- 483            motion: A review. *Sci. Atmos. Sin.*, **22**, 1–12.
- 484    Wang, C.-C., Y.-H. Chen, H.-C. Kuo, S.-Y. Huang, 2013: Sensitivity of typhoon track
- 485            to asymmetric latent heating/rainfall induced by Taiwan topography: A numerical
- 486            study of Typhoon Fanapi (2010). *Journal of Geophysical Research: Atmospheres*
- 487            **118**, 3292–3308.
- 488    Wang, Y., and G. J. Holland, 1996a: The beta drift of baroclinic vortices. Part I:



- 489           Adiabatic vortices. *J. Atmos. Sci.*, **53**, 411–427.
- 490   Wang, Y., and G. J. Holland, 1996b: The beta drift of baroclinic vortices. Part
- 491           II: Diabatic vortices. *J. Atmos. Sci.*, **53**, 3737–3756.
- 492   Wang, Y., and G. J. Holland, 1996c: Tropical cyclone motion and evolution in vertical
- 493           shear. *J. Atmos. Sci.*, **53**, 3313–3332.
- 494   Willoughby, H., 1988: Linear motion of a shallow-water, barotropic vortex. *J. Atmos.*
- 495           *Sci.*, **45**, 1906–1928.
- 496   Wu, C.-C., and K. A. Emanuel, 1993: Interaction of a baroclinic vortex with
- 497           background shear: Application to hurricane movement. *J. Atmos. Sci.*, **50**, 62–76.
- 498   Wu, C.-C., and K. A. Emanuel, 1995a: Potential vorticity diagnostics of hurricane
- 499           movement. Part I: A case study of Hurricane Bob (1991). *Mon. Wea. Rev.*, **123**,
- 500           69–92.
- 501   Wu, C.-C., and K. A. Emanuel, 1995b: Potential vorticity diagnostics of hurricane
- 502           movement. Part II: Tropical Storm Ana (1991) and Hurricane Andrew (1992).
- 503           *Mon. Wea. Rev.*, **123**, 93–109.
- 504   Wu, L., and B. Wang, 2000: A potential vorticity tendency diagnostic approach for
- 505           tropical cyclone motion. *Mon. Wea. Rev.*, **128**, 1899–1911.
- 506   Wu, L., and B. Wang, 2001a: Movement and vertical coupling of adiabatic baroclinic
- 507           tropical cyclones. *J. Atmos. Sci.*, **58**, 1801–1814.
- 508   Wu, L., and B. Wang, 2001b: Effects of convective heating on movement and vertical
- 509           coupling of tropical cyclones: A numerical study. *J. Atmos. Sci.*, **58**, 3639–3649.
- 510   Wu, L., J. Liang, and C.-C. Wu, 2011a: Monsoonal Influence on Typhoon Morakot

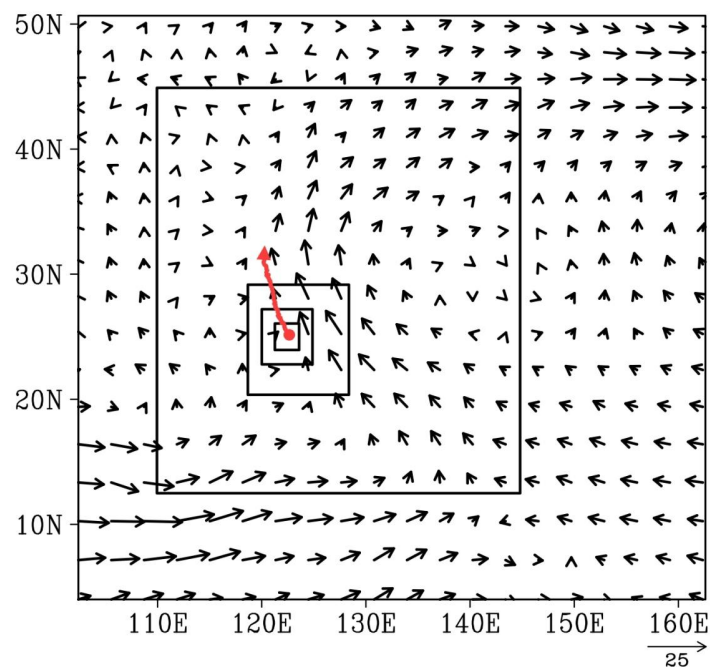


- 511 (2009). Part I: Observational analysis. *J. Atmos. Sci.*, 2208–2221.
- 512 Wu, L., H. Zong, and J. Liang, 2011b: Observational analysis of sudden tropical  
513 cyclone track changes in the vicinity of the East China Sea. *J. Atmos. Sci.*, **68**,  
514 3012–3031.
- 515 Wu, L., S. A. Braun, J. Halverson, and G. Heymsfield, 2006: A numerical study of  
516 Hurricane Erin (2001). Part I: Model verification and storm evolution. *J. Atmos.*  
517 *Sci.*, **63**, 65–86.
- 518 Yu, H., W. Huang, Y. H. Duan, J. C. L. Chan, P. Y. Chen, R. L. Yu. (2007) A  
519 simulation study on pre-landfall erratic track of typhoon Haitang (2005).  
520 *Meteorology and Atmospheric Physics*, **97**, 189-206.
- 521
- 522
- 523





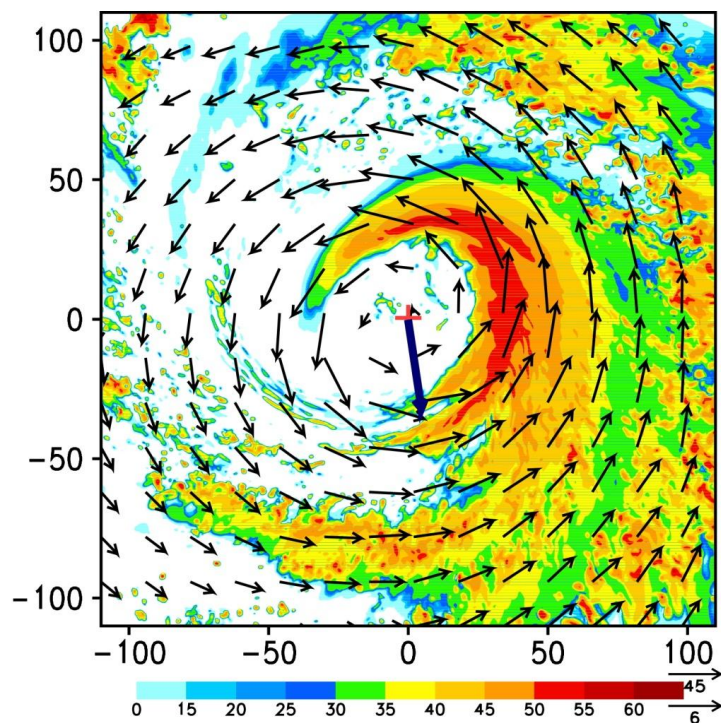
524  
525



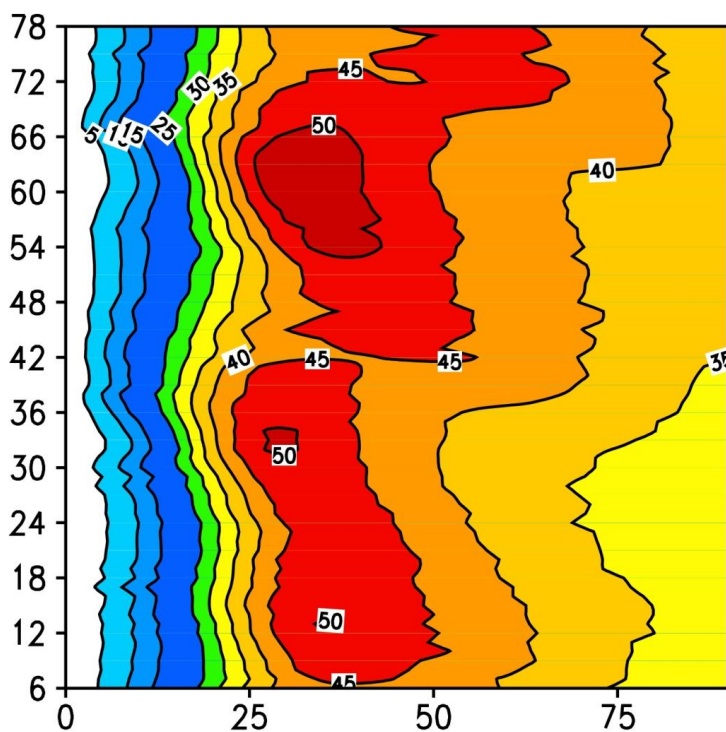
526

527 Figure 1 Model domains of the numerical experiment with the three innermost  
528 domains moving with the storm, the initial 850-hPa wind ( $\text{m s}^{-1}$ ) field (vectors), and  
529 the simulated tropical cyclone track (red)

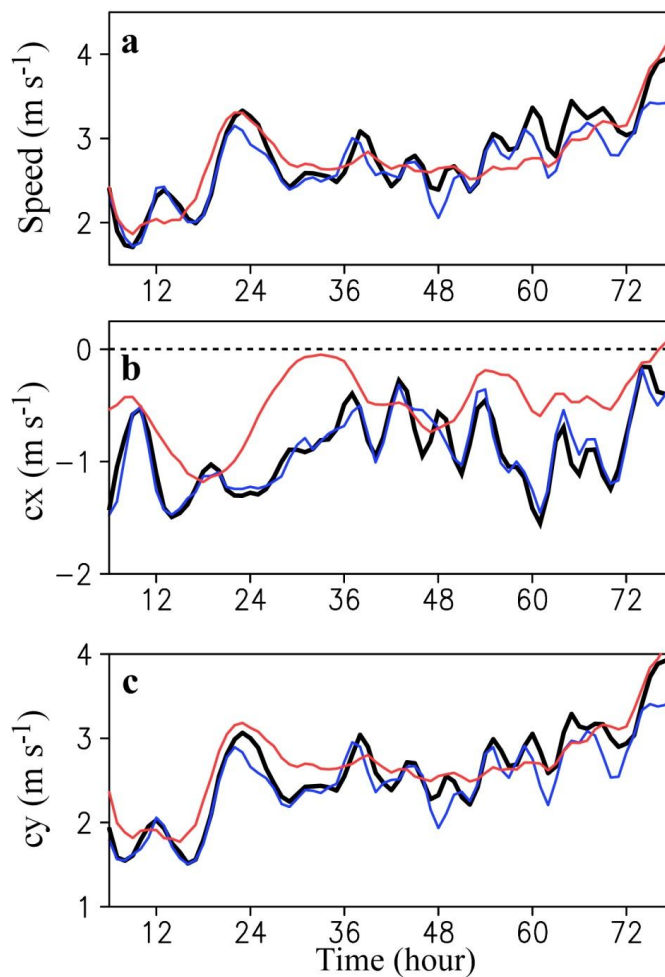
530



531  
532 Figure 2 Simulated wind (vectors,  $\text{m s}^{-1}$ ), radar reflectivity (shading, dBz) fields, and  
533 the vertical wind shear between 200 hPa and 850 hPa over a radius of 500 km from  
534 the tropical cyclone center at 700 hPa after 24-h integration. The labels on the x and y  
535 axes indicate the distance (km) relative to the storm center.



536  
537 Figure 3 Evolution of the simulated azimuthal mean component ( $\text{m s}^{-1}$ ) of the 700-hPa  
538 wind in the 9-km domain. The x-axis and y-axis indicate the distance (km) from the  
539 storm center and the integration time (hours).



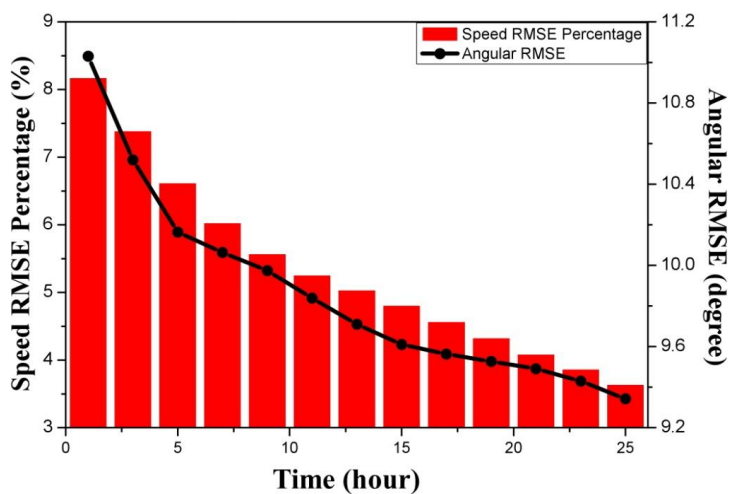
540

541 Figure 4 Time series of tropical cyclone speed (thick black), PVT speed (blue) and

542 conventional steering (red): a) magnitude, b) zonal component, and c) meridional

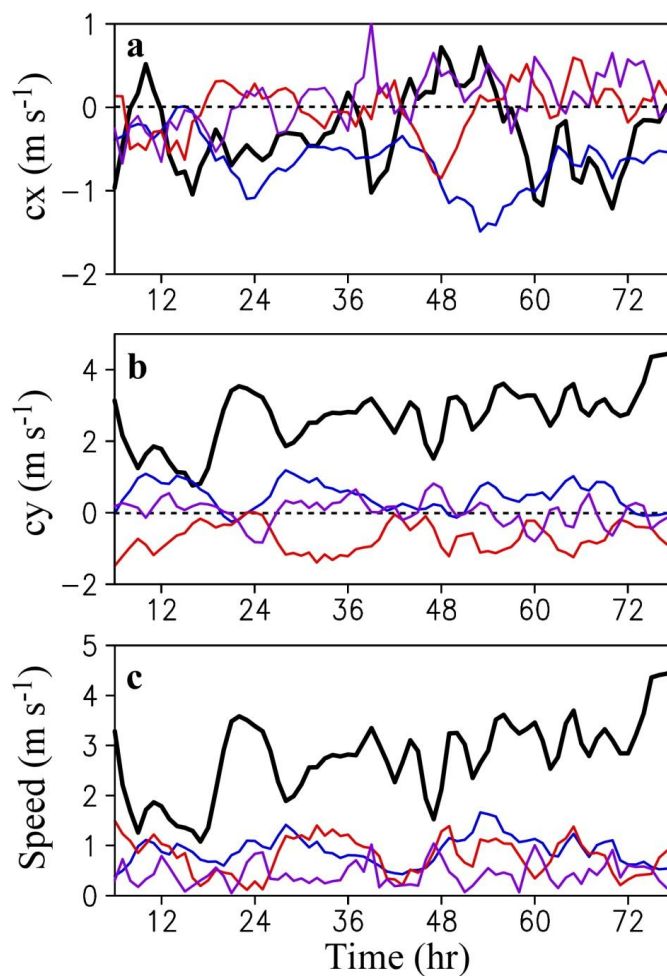
543 component

544



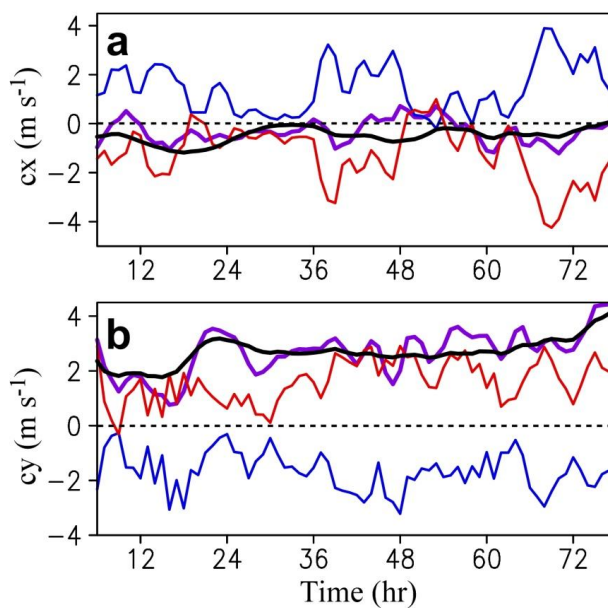
545

546 Figure 5 Changes of the RMSEs of the speed (right, %) and direction (left, °) of the  
547 conventional steering with various average periods



548

549 Figure 6 Contributions of the horizontal advection (HA, black), vertical advection  
550 (VA, blue), diabatic heating (DH, red) and friction (FR, purple) terms in the PVT  
551 equation to tropical cyclone motion: a) zonal component, b) meridional component,  
552 and c) magnitude

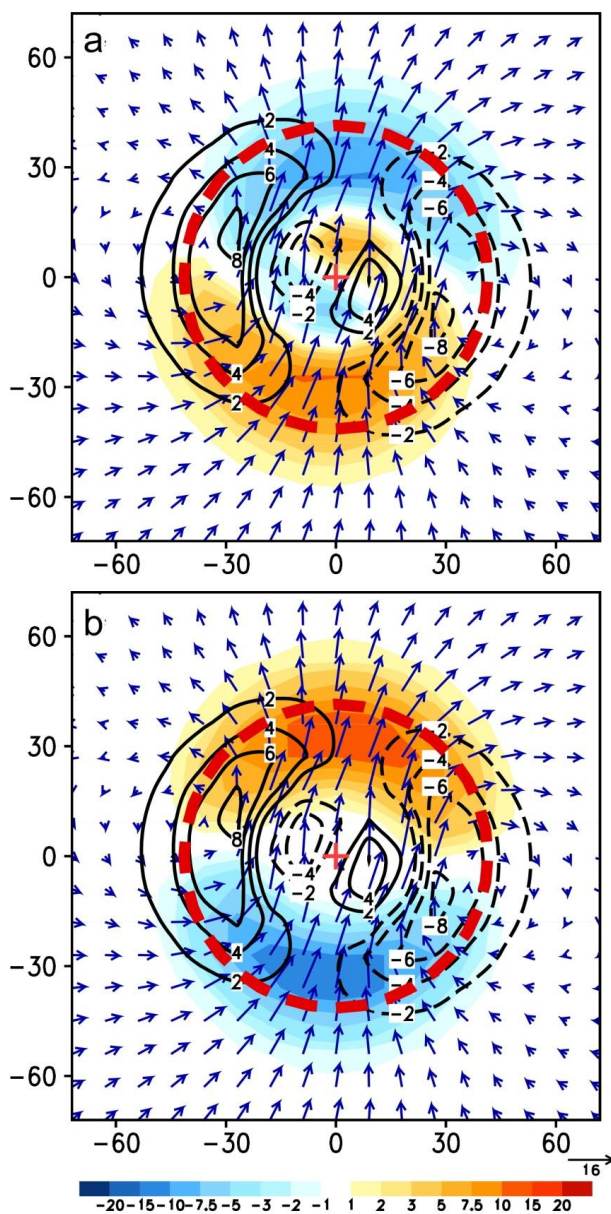


553

554 Figure 7 Time series of the conventional steering (thick black) and the contributions

555 of the HA (thick purple) and the HA1 (red) and HA2 (blue) terms. The conventional

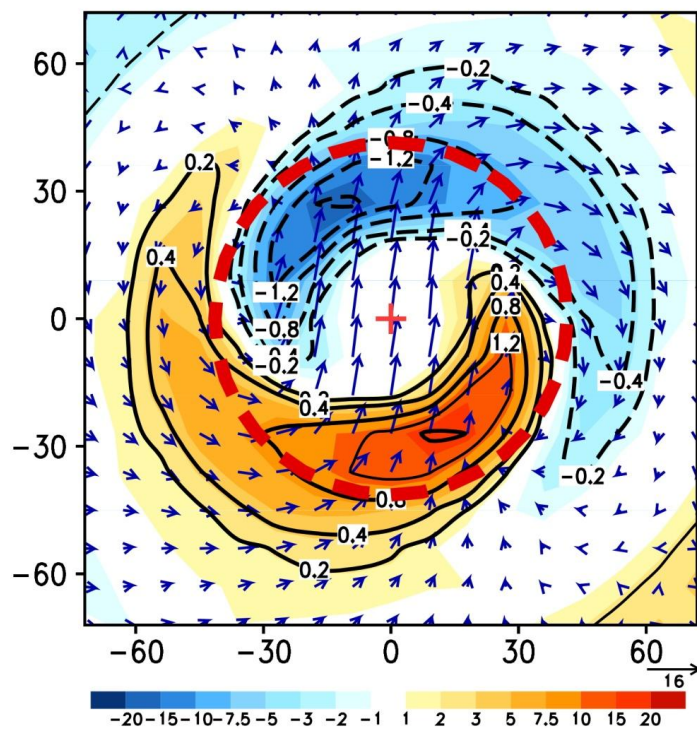
556 steering is deduced from the contribution of the HA1 term.



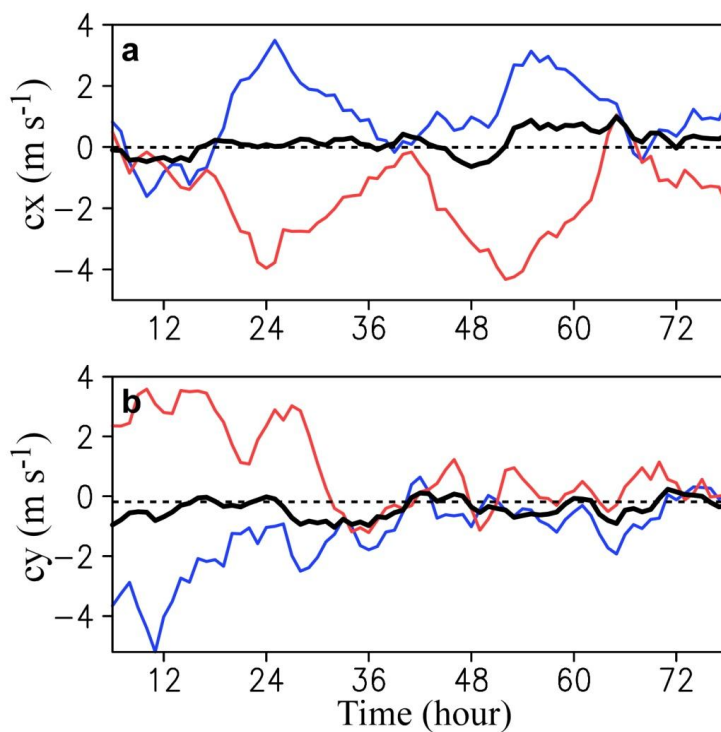
557

558 Figure 8 (a) HA1 (shaded,  $10^{-10} \text{ s}^{-2}$ ) and (b) HA2 (shaded,  $10^{-10} \text{ m}^2 \text{ s}^{-2} \text{ K kg}^{-1}$ ) with the  
559 wavenumber-one components of potential vorticity (contours,  $10^{-6} \text{ m}^2 \text{ s}^{-1} \text{ K kg}^{-1}$ ) and  
560 winds (vectors,  $\text{m s}^{-1}$ ) at 700 hPa after 18 hours of integration. The dashed circle  
561 indicates the radius of maximum wind.

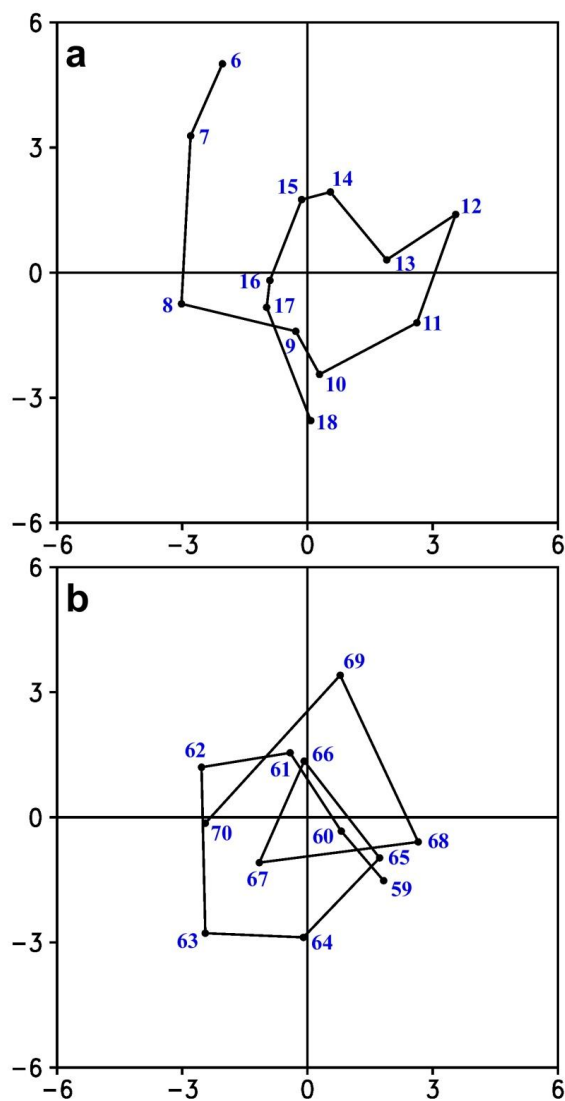




562  
563 Figure 9 The wavenumber-one components of the 500-hPa vertical motion (contours,  
564  $\text{m s}^{-1}$ ), 700-hPa winds relative to the tropical cyclone motion (vectors,  $\text{m s}^{-1}$ ), and  
565 500-hPa heating rate (shaded,  $10^{-4} \text{ K s}^{-1}$ ) after 18 hours of integration. The dashed  
566 circle indicates the radius of maximum wind.



567  
568 Figure 10 Time series of the contributions of diabatic heating at 700 hPa (blue) and  
569 400 hPa (red) and the contribution of daiabtic heating (thick black) averaged over the  
570 layer between 300 hPa and 850 hPa

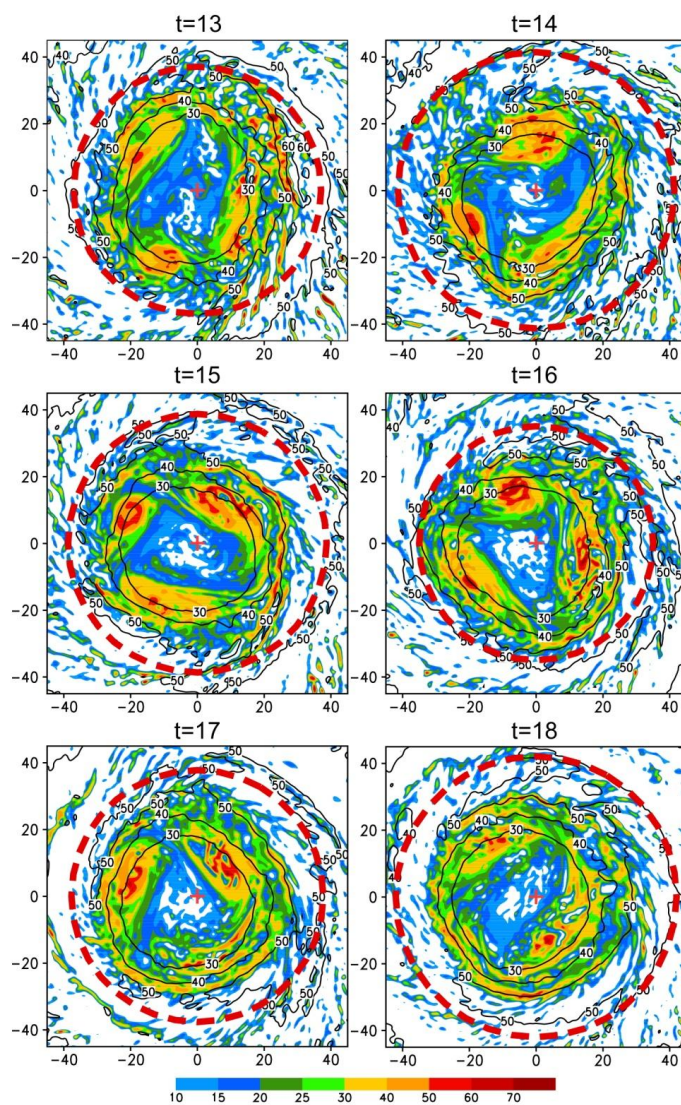


571

572 Figure 11 Small-amplitude oscillation of the tropical cyclone track with respect to the

573 9-hour running mean track: a) 6-18 h and b) 59-69 h

574

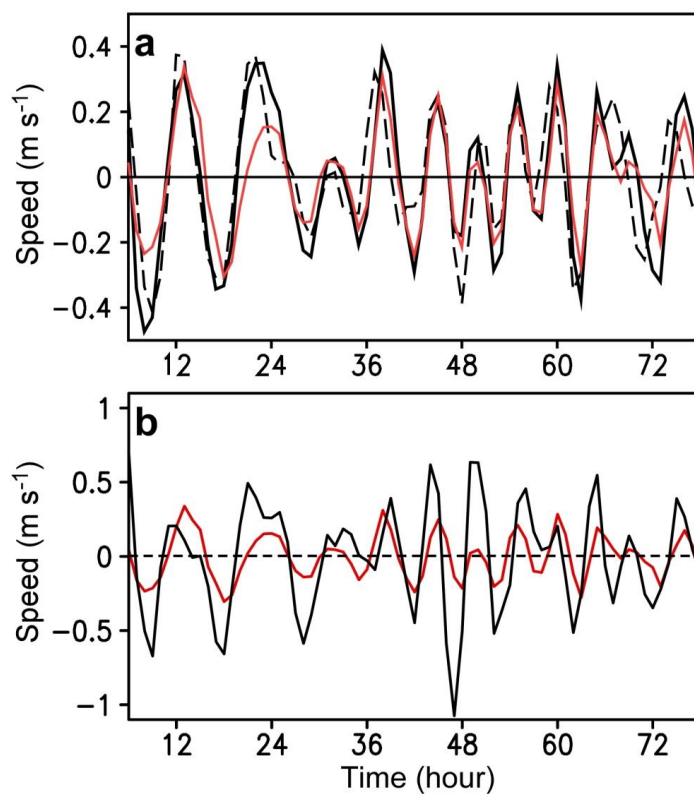


575

576 Figure 12 Distribution of potential vorticity ( $10^{-6} \text{ m}^2 \text{ s}^{-1} \text{ K kg}^{-1}$ ) within inner-core  
577 region during 13-18 h. The dashed circle shows the radius of maximum wind with the  
578 tropical cyclone center indicating with crosses.

579

580



581

582

583 Figure 13 Fluctuations of (a) the tropical cyclone speed (black solid), the PVT speed

584 (black dashed) and the difference between the tropical cyclone speed and the

585 conventional steering (red solid), and (b) the difference between the tropical cyclone

586 speed and the conventional steering (red solid), and the difference between the

587 contribution of the HA term and the conventional steering (black).

588

589